Acta Mechanica Sinica (2014) 30(5):615–627
DOI 10.1007/s10409-014-0038-5

RESEARCH PAPER

Low-thrust trajectory optimization in a full ephemeris model

Xing-Shan Cai · Yang Chen · Jun-Feng Li

Received: 28 October 2013 / Revised: 13 January 2014 / Accepted: 24 February 2014

Abstract The low-thrust trajectory optimization with complicated constraints must be considered in practical engineering. In most literature, this problem is simplified into a two-body model in which the spacecraft is subject to the gravitational force at the center of mass and the spacecraft's own electric propulsion only, and the gravity assist (GA) is modeled as an instantaneous velocity increment. This paper presents a method to solve the fuel-optimal problem of low-thrust trajectory with complicated constraints in a full ephemeris model, which is closer to practical engineering conditions. First, it introduces various perturbations, including a third body's gravity, the nonspherical perturbation and the solar radiation pressure in a dynamic equation. Second, it builds two types of equivalent inner constraints to describe the GA. At the same time, the present paper applies a series of techniques, such as a homotopic approach, to enhance the possibility of convergence of the global optimal solution.

Keywords Low-thrust · Full ephemeris model · Gravity assist

1 Introduction

Electric propulsion has attracted much attention in the past few decades. Compared with traditional chemical propulsion, electric propulsion can efficiently reduce the fuel consumption due to a higher specific impulse [1, 2]. Electric propulsion was first used in the Deep Space mission 1 [3] and demonstrated its appeal in the recently successful Hayabusa return mission [4]. Combined with the technique of planetary gravity assist (GA), electric propulsion is usually a preferred propulsion for future interplanetary missions. Much research has been conducted on low-thrust trajectory optimization, the methods of which are typically categorized into [5] direct methods [6, 7], indirect methods [8, 9] and combinations of these two, which are termed hybrid methods [10, 11]. The present paper is based on indirect methods. The indirect methods are always used to solve two-point boundary-value problems (TPBVPs) derived from the calculus of variations and Pontryagin's maximum principle (PMP). However, with small convergence radii, the sensitive initial guesses and the fussy formula derivations with complex constraints, the solutions of shooting functions corresponding to TPBVPs are rather difficult to achieve. In addition, the discontinuous control (bang-bang control [12–14]) can also lead to bad integral accuracy.

The fuel consumption is large when the target is far away from the Earth. In many missions, GA is also used to reduce the fuel consumption, a technique that has been applied in many missions. GA was initially studied for the engineering mission, and some typical GA sequences were gradually presented. The most typical example, Jupiter's Galileo, used an EVEEJ sequence [15], and the craft finally arrived at Jupiter with a low cost. The GA was later analyzed theoretically. Broucke et al. [16] used linked conics in a two-body model and gave the flyby maneuver to increase or decrease the orbit energy. Prado et al. [17] gave the measure of the GA time via a combination of the impulsive maneuver and the GA. Felipe et al. [18, 19] sorted the trajectory by analyzing the mechanical energy of the spacecraft and the GA planet. Strange et al. [20] proposed the method to search for the GA sequence by analyzing the energies of the spacecraft and the planet. All the researches above treated the GA in the linked-conics model (two-body model), in which the GA planet was considered as massless and the GA was modeled as an instantaneous velocity increment. The work to study the GA via a full ephemeris model is scarce. Bayliss [21] studied the GA by considering the third body's gravity perturbation in a two-body model, which did not avoid linking the trajectory, and the procedure was very complicated.

After the primary design in a two-body model, three challenging problems have to be faced. On the one hand, in the real deep space environment, the spacecraft is subject

X.-S. Cai · Y. Chen · J.-F. Li (✉)
School of Aerospace, Tsinghua University,
100084 Beijing, China
e-mail: lijunf@tsinghua.edu.cn

to various perturbations that have influences and can not be ignored during the long travel. On the other hand, the gravity of a GA planet can not be neglected but is instead the main factor when flying through the sphere of planetary influence, so the GA in the two-body model can not describe the real GA process. Finally, is the simplification of the two-body model that is commonly used reasonable, and does the design have a reference value? This paper provides answers to these three problems. First, the present paper gives a further trajectory design that considers complicated constraints, which is closer to the practical space environment. The paper introduces various main perturbations, including the third body's gravity, the nonspherical perturbation and the solar radiation pressure, which strengthen the nonlinearity of the dynamic equation, and derives the first-order necessary conditions of optimal control. Second, the present paper builds two sets of 3-D equivalent inner equality constraints to describe the GA. The first type of the constraints constrains the actual orbit inclination, the perigee distance and the true anomaly relative to the GA planet. The second type of the constraints constrains the B-plane parameters and the true anomaly relative to the GA planet. Finally, the present paper compares the two-body model and the full ephemeris model and assesses the reference value of the two-body model. At the same time, the present paper applies a series of techniques to enhance the possibility of convergence of the global optimal solution, including, among others, the homotopic approach method [22, 23].

The remainder of the present paper is organized as follows: the second section discusses TPBVPs in the full ephemeris model, which introduces the gravity of the third body, the nonspherical perturbation and the solar radiation pressure in a dynamic equation, and derives the first-order necessary conditions of optimal control. The third section discusses the problem in which the spacecraft departs from Asteroid 1 and targets Asteroid 2 in the full model with a single GA from the Earth and builds two types of inner constraints to describe the GA. The fourth section presents two numerical examples using the method presented in Sect. 2 and Sect. 3 and gives a comparative analysis of the two-body model and the full ephemeris model. Conclusions are drawn in the last section.

2 The low-thrust trajectory optimization in a full ephemeris model

In the research of the low-thrust trajectory optimization problem, a heliocentric two-body model is commonly used to reduce the number of numerical calculations; this model assumes that the spacecraft is subject only to the central force of the Sun's gravity and the force of the craft's own electric propulsion system. In a practical space environment, the spacecraft is also subject to various perturbations, which can cause obvious deviations due to these perturbations' long-term effects. It is therefore necessary to research the low-thrust trajectory optimization in a full ephemeris model, which contains the planetary gravity perturbation of a third body, the solar radiation pressure perturbation and the nonspherical perturbation. This paper takes a heliocentric two-body trajectory as an example to check the design method in a full ephemeris model.

2.1 The perturbations in a full ephemeris model

To research the low-thrust heliocentric transfer trajectory, the main perturbation forces are the planetary gravity perturbation, the solar radiation pressure perturbation and the nonspherical perturbation.

2.1.1 Planetary gravity perturbation

In the heliocentric transfer trajectory, the spacecraft is subject to not only the Sun's gravity but also the planetary gravity. In the heliocentric ecliptic reference frame (HERF), the third-body gravity perturbative acceleration $\boldsymbol{f}_{\mathrm{Pl}}$ is

$$\boldsymbol{f}_{\mathrm{Pl}} = -\frac{\mu_{\mathrm{Pl}}}{\|\boldsymbol{r}-\boldsymbol{r}_{\mathrm{Pl}}\|^3}(\boldsymbol{r}-\boldsymbol{r}_{\mathrm{Pl}}) - \frac{\mu_{\mathrm{Pl}}}{\|\boldsymbol{r}_{\mathrm{Pl}}\|^3}\boldsymbol{r}_{\mathrm{Pl}}, \tag{1}$$

where $\boldsymbol{r}$ and $\boldsymbol{r}_{\mathrm{Pl}}$ denote the positions of the spacecraft and the planet in the HERF, respectively. μ_{Pl} denotes the gravitational constant of the planet.

2.1.2 Solar radiation pressure perturbation

Because the area of the solar cell panels of the electric propulsion spacecraft is large, the solar radiation pressure is one of the main disturbing forces. Suppose that the solar cell panels are always facing the Sun; the solar radiation pressure acceleration $\boldsymbol{f}_{\mathrm{Solar}}$ can be written as

$$\boldsymbol{f}_{\mathrm{Solar}} = \frac{(1+\eta)SL_0}{c}\frac{\boldsymbol{r}}{mr^3} = \beta\frac{\boldsymbol{r}}{mr^3}, \tag{2}$$

where $\eta \in [0,1]$ denotes the reflection coefficient of the spacecraft's surface. S denotes the area of the spacecraft's surface. L_0 is the solar flux near Earth. c is the speed of light. m is the instantaneous mass of the spacecraft. All the variables are constants except $\boldsymbol{r}$ and m, and $\beta = (1+\eta)SL_0/c$ is called the solar radiation pressure factor.

2.1.3 Nonspherical perturbation

When the spacecraft is swinging in the main planet's sphere of influence, departing from the main planet or targeting the main planet, nonspherical perturbations can not be ignored. Because the time in the main planet's sphere of influence is short, the influence of the nonspherical perturbation is tiny. Only the largest factor J_2 is considered. The nonspherical perturbation $\boldsymbol{f}_{\mathrm{C}}$ is

$$\boldsymbol{f}_{\mathrm{C}} = -\frac{\mu_{\mathrm{Pl}}r_0^2J_2}{2}\Big(-\frac{15\boldsymbol{r}\sin^2\varphi}{r^5} + \frac{3\boldsymbol{r}}{r^5} + \frac{6\sin\varphi}{r^4}\frac{\partial z}{\partial \boldsymbol{r}}\Big), \tag{3}$$

where ϕ denote the geocentric dimension and $\partial z/\partial \boldsymbol{r} = [0\ \ 0\ \ 1]^{\mathrm{T}}$. All variables are projected in the equatorial coordinate system of the planet.

2.2 Problem statement

The dynamic equations of a low-thrust trajectory can be writ-

ten as

$$\begin{aligned}\dot{\boldsymbol{r}} &= \boldsymbol{v},\\ \dot{\boldsymbol{v}} &= -\frac{\mu}{r^3}\boldsymbol{r} + \sum \boldsymbol{f}_{\mathrm{Pl}} + \boldsymbol{f}_{\mathrm{Solar}} + \boldsymbol{f}_{\mathrm{C}} + \frac{T_{\max}u}{m}\boldsymbol{\alpha},\\ \dot{m} &= -\frac{T_{\max}}{I_{\mathrm{sp}}g_0}u,\end{aligned} \tag{4}$$

where $\boldsymbol{v}$ denotes the velocity vectors in the HERF. μ denotes the Sun's gravitational constant, $1.327\,124\,400\,18\times10^{11}\,\mathrm{km^3/s^2}$. The control variables consist of $\boldsymbol{\alpha}$, the unit vector of the thrust direction, and $u\in[0,1]$, the ratio of the practical thrust to the maximum thrust. $T_{\max}$ and I_{sp} are the maximum thrust magnitude and the thruster-specific impulse of the onboard engine. g_0 is the standard acceleration of gravity at sea level, 9.806 65 m/s. The quantities $T_{\max}$, I_{sp}, and g_0 are customarily in international units. $\sum \boldsymbol{f}_{\mathrm{Pl}}$ are the perturbations of all third bodies, mainly the eight main planets.

The fuel-optimal control problem is to maximize the final mass of the spacecraft or to minimize the fuel consumption expressed by

$$J = \frac{T_{\max}}{I_{\mathrm{sp}}g_0}\int_{t_0}^{t_{\mathrm{f}}} u\mathrm{d}t. \tag{5}$$

To study an interplanetary trajectory, the scenario of the spacecraft departing from Earth at the sphere of influence, with a hyperbolic excess velocity vector $\boldsymbol{v}_\infty$ provided by the launch vehicle, is considered. The initial states of the spacecraft can therefore be written as

$$\boldsymbol{r}(t_0) = \boldsymbol{r}_{\mathrm{E}}(t_0) + \boldsymbol{r}_\infty, \quad \boldsymbol{v}(t_0) = \boldsymbol{v}_{\mathrm{E}}(t_0) + v_\infty, \quad m(t_0) = m_0, \tag{6}$$

where t_0 is the launch time. $\boldsymbol{r}_{\mathrm{E}}(t_0)$ and $\boldsymbol{v}_{\mathrm{E}}(t_0)$ are the position vector and the velocity vector of Earth at t_0, respectively. $\boldsymbol{r}_\infty$ is the position vector pointing from Earth to the sphere of influence, and $\boldsymbol{v}_\infty$ is the escape velocity vector. The 6-D equality constraints correspond to Lagrange numerical multipliers $\boldsymbol{\chi}_{1-6}$.

The final conditions are the Asteroid rendezvous conditions

$$\boldsymbol{r}(t_{\mathrm{f}}) = \boldsymbol{r}_{\mathrm{As}}(t_{\mathrm{f}}), \quad \boldsymbol{v}(t_{\mathrm{f}}) = \boldsymbol{v}_{\mathrm{As}}(t_{\mathrm{f}}), \tag{7}$$

where t_{f} is the final time. $\boldsymbol{r}_{\mathrm{As}}(t_{\mathrm{f}})$ and $\boldsymbol{v}_{\mathrm{As}}(t_{\mathrm{f}})$ are the position and velocity vectors of the target Asteroid at t_{f}. The 6-D equality constraints correspond to Lagrange numerical multipliers $\boldsymbol{\chi}_{7-14}$.

By introducing the costate vectors $\boldsymbol{\lambda} = [\boldsymbol{\lambda}_r, \boldsymbol{\lambda}_v, \lambda_m]^{\mathrm{T}}$, the Hamiltonian can be given as

$$\begin{aligned}H = \frac{T_{\max}}{I_{\mathrm{sp}}g_0}u + \boldsymbol{\lambda}_r\cdot\boldsymbol{v} + \boldsymbol{\lambda}_v\cdot\Big(-\frac{\mu}{r^3}r + \sum \boldsymbol{f}_{\mathrm{Pl}} + \boldsymbol{f}_{\mathrm{Solar}}\\ + \boldsymbol{f}_{\mathrm{C}} + \frac{T_{\max}u}{m}\boldsymbol{\alpha}\Big) - \lambda_m\frac{T_{\max}}{I_{\mathrm{sp}}g_0}u.\end{aligned} \tag{8}$$

The optimal direction and the magnitude of the thrust vector, which should minimize the Hamiltonian using PMP, are then determined by

$$\boldsymbol{\alpha} = -\frac{\boldsymbol{\lambda}_v}{\|\boldsymbol{\lambda}_v\|}, \tag{9}$$

$$\begin{aligned}u &= 0, && \text{if } \rho > 0,\\ u &= 1, && \text{if } \rho < 0,\\ 0 &\leqslant u \leqslant 1, && \text{if } \rho = 0,\end{aligned} \tag{10}$$

where ρ is called the switch function, which has the form of

$$\rho = 1 - \frac{I_{\mathrm{sp}}g_0\,\|\boldsymbol{\lambda}_v\|}{m} - \lambda_m, \tag{11}$$

The costate differential functions can be derived as

$$\begin{aligned}\dot{\boldsymbol{\lambda}}_r &= \frac{\mu\boldsymbol{\lambda}_v}{r^3} - \frac{3\mu\boldsymbol{r}\boldsymbol{\lambda}_v\boldsymbol{r}}{r^5} - \sum\frac{\partial(\boldsymbol{\lambda}_v\boldsymbol{f}_{\mathrm{Pl}})}{\partial\boldsymbol{r}}\\ &\quad -\frac{\partial(\boldsymbol{\lambda}_v f_{\mathrm{Solar}})}{\partial\boldsymbol{r}} - \frac{\partial(\boldsymbol{\lambda}_v f_C)}{\partial\boldsymbol{r}},\\ \dot{\boldsymbol{\lambda}}_v &= -\boldsymbol{\lambda}_r,\\ \dot{\lambda}_m &= -\frac{T_{\max}u\,\|\boldsymbol{\lambda}_v\|}{m^2} - \frac{\partial(\boldsymbol{\lambda}_v f_{\mathrm{Solar}})}{\partial m},\end{aligned} \tag{12}$$

where

$$\begin{aligned}\frac{\partial(\boldsymbol{\lambda}_v\boldsymbol{f}_{\mathrm{Pl}})}{\partial\boldsymbol{r}} &= \frac{\mu_{\mathrm{Pl}}\boldsymbol{\lambda}_v}{\|\boldsymbol{r}-\boldsymbol{r}_{\mathrm{Pl}}\|^3} + \frac{3\mu_{\mathrm{Pl}}\boldsymbol{\lambda}_v(\boldsymbol{r}-\boldsymbol{r}_{\mathrm{Pl}})}{\|\boldsymbol{r}-\boldsymbol{r}_{\mathrm{Pl}}\|^5}(\boldsymbol{r}-\boldsymbol{r}_{\mathrm{Pl}}),\\ \frac{\partial(\boldsymbol{\lambda}_v\cdot\boldsymbol{f}_{\mathrm{Solar}})}{\partial\boldsymbol{r}} &= \beta\Big(\frac{\boldsymbol{\lambda}_v}{mr^3} - \frac{3\boldsymbol{\lambda}_v\cdot\boldsymbol{r}}{r^5}\boldsymbol{r}\Big),\\ \frac{\partial(\boldsymbol{\lambda}_v\boldsymbol{f}_{\mathrm{Solar}})}{\partial m} &= -\beta\frac{\boldsymbol{\lambda}_v\cdot\boldsymbol{r}}{m^2r^3},\\ \frac{\partial(\boldsymbol{\lambda}_v\boldsymbol{f}_{\mathrm{C}})}{\partial\boldsymbol{r}} &= \frac{15\mu r_0^2J_2}{2}\Big[\frac{\sin^2\varphi}{r^5}\boldsymbol{\lambda}_v - \frac{7\sin^2\varphi(\boldsymbol{\lambda}_v\boldsymbol{r})}{r^7}\boldsymbol{r}\\ &\quad + \frac{2\sin\varphi(\boldsymbol{\lambda}_v\boldsymbol{r})}{r^6}\frac{\partial z}{\partial\boldsymbol{r}}\Big]\\ &\quad -\frac{\mu r_0^2J_2}{2}\Big[\frac{3}{r^5}\boldsymbol{\lambda}_v - 15\frac{(\boldsymbol{\lambda}_v\boldsymbol{r})}{r^7}\boldsymbol{r}\Big]\\ &\quad -3\mu r_0^2J_2\Big(\boldsymbol{\lambda}_v\frac{\partial z}{\partial\boldsymbol{r}}\Big)\Big(-\frac{5\sin\varphi}{r^6}\boldsymbol{r} + \frac{1}{r^5}\frac{\partial z}{\partial\boldsymbol{r}}\Big).\end{aligned} \tag{13}$$

As in Eq. (3), the variables in Eq. (13) are projected in the equatorial coordinate system of the planet.

According to the transversal conditions, when the boundary state is fixed, the corresponding boundary costate is free, and when the former is free, the latter is fixed. The initial position and velocity constraints are time dependent, so the initial costate vectors and the final transversal conditions should satisfy

$$\boldsymbol{\lambda}_{r,v}(t_0) + \boldsymbol{\chi}_{1-6} = \boldsymbol{0}, \tag{14}$$

$$-\boldsymbol{\lambda}_{r,v}(t_{\mathrm{f}}) + \boldsymbol{\chi}_{7-12} = \boldsymbol{0}, \tag{15}$$

$$\lambda_m(t_{\mathrm{f}}) = 0. \tag{16}$$

For convenience, in the numerical solution process, $\boldsymbol{\chi}_{1-12}$ is expressed with $\boldsymbol{\lambda}_r(t_0)$, $\boldsymbol{\lambda}_v(t_0)$, $\boldsymbol{\lambda}_r(t_{\mathrm{f}})$, and $\boldsymbol{\lambda}_v(t_{\mathrm{f}})$ via Eqs. (14) and (15). Therefore, the Lagrange numerical multipliers $\boldsymbol{\chi}_{1-12}$ do not appear in the shooting functions.

The final stationary conditions are derived as

$$-H(t_0) - \boldsymbol{\chi}_{1-3} \cdot \boldsymbol{v}_{\mathrm{E}}(t_0) - \boldsymbol{\chi}_{4-6} \cdot \boldsymbol{a}_{\mathrm{E}}(t_0) = 0, \tag{17}$$

$$H(t_{\mathrm{f}}) - \boldsymbol{\chi}_{7-9} \cdot \boldsymbol{v}_{\mathrm{As}}(t_{\mathrm{f}}) - \boldsymbol{\chi}_{10-12} \cdot \boldsymbol{a}_{\mathrm{As}}(t_{\mathrm{f}}) = 0. \tag{18}$$

It is clear that there are nine unknowns, including the 7-D initial values of the costate vectors $\lambda(t_0)$ and the 2-D initial time t_0 and final time t_{f}. At the same time, there are the same number of equations, including the 6-D rendezvous conditions (7), the 1-D transversal condition (16), and the 2-D stationary condition (17) and (18).

3 The low-thrust trajectory optimization with GA in a full ephemeris model

In the research of a trajectory design with GA, the heliocentric transfer trajectory is usually modeled with a two-body model. For convenience, the effect of planetary GA is modeled as an instantaneous velocity increment of the spacecraft at the event time, showed in Fig. 1a. At the event time, it is constrained that the position of the spacecraft $\boldsymbol{r}(t_m)$ to be the same as that of the GA planet $\boldsymbol{r}_{\mathrm{Pl}}(t_m)$, the incoming hyperbolic excess speed $\boldsymbol{v}_{\infty}^{-}$ is equal to the outgoing speed $\boldsymbol{v}_{\infty}^{+}$, and the rotation angle θ should not be greater than the maximum rotation angle $\theta_{\max}$. This result is acceptable in an initial trajectory design.

In the practical mission, the GA is not one instantaneous process but is instead a continuous process, showed in Fig. 1b. The spacecraft approaches the GA planet gradually and flies mainly under the GA planet's gravity in the planet's sphere of influence for several days. During the flyby process, the states of the spacecraft are continuous. After the GA process, the states of the spacecraft are different from the result designed with a two-body model, which can result in a large error after the following flight. The instantaneous incremental velocity model can not satisfy the precision requirement.

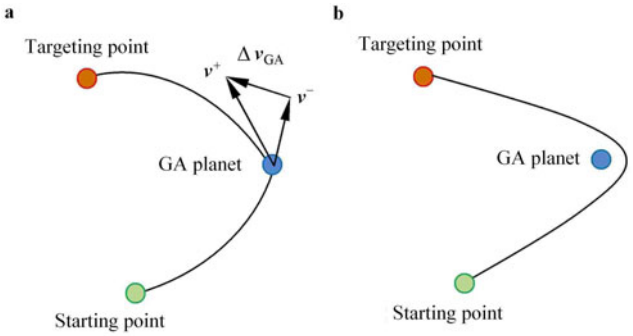

Fig. 1 **a** GA in a two-body model; **b** GA in a full ephemeris model

This section considers the low-thrust trajectory with a single GA using a full ephemeris model, and builds two types of equivalent inner constraints, that can accurately describe the GA process, to achieve the GA effect, which can change the states of the spacecraft freely.

3.1 Boundary conditions

The techniques presented in the preceding section are used in this complex case involving inner constraints. The dynamic equations are the same as Eq. (4). The performance index and the Hamiltonian are the same as Eqs. (5) and (8). The optimal direction and the magnitude of the thrust vector are the same as Eqs. (9)–(11). The costate differential equations are the same as Eq. (12).

The optimal control problem with a fixed boundary only is considered as well. The spacecraft is considered that starts from Asteroid 1 with the same velocity vectors as the Asteroid 1 at a fixed time t_0, and is then flying by a GA planet to obtain a GA, and finally targets Asteroid 2. The initial states and the final states of the spacecraft can therefore be written as

$$\boldsymbol{r}(t_0) = \boldsymbol{r}_{\mathrm{As1}}(t_0), \quad \boldsymbol{v}(t_0) = \boldsymbol{v}_{\mathrm{As1}}(t_0), \quad m(t_0) = m_0, \tag{19}$$

$$\boldsymbol{r}(t_{\mathrm{f}}) = \boldsymbol{r}_{\mathrm{As2}}(t_{\mathrm{f}}), \quad \boldsymbol{v}(t_{\mathrm{f}}) = \boldsymbol{v}_{\mathrm{As2}}(t_{\mathrm{f}}), \tag{20}$$

where $\boldsymbol{r}_{\mathrm{As1}}(t_0)$ and $\boldsymbol{v}_{\mathrm{As1}}(t_0)$ are the position vector and the velocity vector of Asteroid 1 at t_0, and $\boldsymbol{r}_{\mathrm{As2}}(t_0)$ and $\boldsymbol{v}_{\mathrm{As2}}(t_0)$ are the position vector and the velocity vector of Asteroid 2 at t_{f}, respectively. These 12-D equality constraints correspond to the Lagrange numerical multipliers $\boldsymbol{\chi}_{1-12}$.

3.2 The inner constraints

The next step is to build inner equality constraints. The trajectory of the spacecraft relative to the GA planet is a hyperbolic curve, which is called the GA hyperbolic. The GA hyperbolic is the constraint of the GA process. The direction and magnitude of the velocity relative to the GA planet are established when the spacecraft arrives at the GA planet's sphere of influence. The hyperbolic can therefore be determined by the time and two other parameters. The time can be expressed by the true anomaly. The two other parameters are of two types. The first type constrains the actual orbit inclination and the perigee distance relative to the GA planet. The second type constrains two B-plane parameters B_{T} and B_{R} relative to the GA planet. Both of these types have 3-D equality constraints, which correspond to the Lagrange numerical multipliers $\boldsymbol{\chi}_{13-15}$. The nominal values of both of the types of inner constraints are given by the two-body model.

3.2.1 First type of inner constraints

The first type of inner constraints is written as

$$\psi^{1}_{13-15} \triangleq \begin{bmatrix} i(t_m) - i_{\mathrm{norm}} = 0 \\ r_{\mathrm{p}}(t_m) - r_{\mathrm{pnorm}} = 0 \\ f(t_m) - f_{\mathrm{norm}} = 0 \end{bmatrix} = 0, \tag{21}$$

where t_m is the time of the perigee of the hyperbolic relative to the GA planet. $i(t_m)$, $r_{\mathrm{p}}(t_m)$, and $f(t_m)$ are the actual orbit inclination, the perigee distance and the true anomaly of the hyperbolic in the full ephemeris model. i_{norm}, r_{pnorm}, and f_{norm} are the nominal orbit inclination, the perigee distance and the true anomaly given by the two-body model. The first

two equations ensure that the spacecraft's states are suitable for the states given by the two-body model at the perigee time, and the last equation ensures that t_m is the time of the perigee of the hyperbolic. Therefore let us set $f_{\text{norm}} = 0$.

3.2.1.1 Nominal orbit inclination and the perigee distance

The nominal orbit inclination and the perigee distance can be defined by the incoming and outgoing hyperbolic residual velocities in the two-body model of the trajectory with GA. The nominal orbit inclination is defined as

$$\cos(i_{\text{norm}}) = n_z \big/ \|\boldsymbol{n}\|, \tag{22}$$

$$\boldsymbol{n} = \frac{\boldsymbol{v}_\infty^- \times \boldsymbol{v}_\infty^+}{|\boldsymbol{v}_\infty^- \times \boldsymbol{v}_\infty^+|}, \quad n_z = \boldsymbol{n} \cdot \boldsymbol{k}, \tag{23}$$

where $\boldsymbol{n}$ is the orbital plane normal to the spacecraft relative to the GA planet and $\boldsymbol{k}$ is the reference unit vector, which is set as the ecliptic plane normal for convenience, $\boldsymbol{k} = (0, 0, 1)^{\text{T}}$.

The nominal perigee distance is defined as

$$r_{\text{pnorm}} = \frac{\mu_{\text{Pl}}}{v_\infty^2}\left[\frac{1}{\sin(\theta/2)} - 1\right], \tag{24}$$

where θ is rotational angle of the hyperbolic excess speed for the planetary GA, which is defined as

$$\sin\frac{\theta}{2} = \sqrt{\frac{1-\cos\theta}{2}}, \quad \cos\theta = \frac{\boldsymbol{v}_\infty^- \cdot \boldsymbol{v}_\infty^+}{v_\infty^2}. \tag{25}$$

3.2.1.2 Actual orbit inclination, the perigee distance and the true anomaly

The actual orbit inclination, the perigee distance and the true anomaly can be calculated from the actual position and velocity vectors relative to the GA planet. The actual orbit inclination is defined as

$$\cos(i(t_m)) = h_z \big/ \|\boldsymbol{h}\|, \tag{26}$$

where $\boldsymbol{h}$ is the angular momentum of the spacecraft relative to the GA planet

$$\boldsymbol{h} = \Delta\boldsymbol{r}(t_m) \times \Delta\boldsymbol{v}(t_m), \quad h_z = \boldsymbol{h} \cdot \boldsymbol{N}, \tag{27}$$

where

$$\Delta\boldsymbol{r}(t_m) = \boldsymbol{r}(t_m) - \boldsymbol{r}_{\text{Pl}}(t_m), \quad \Delta\boldsymbol{v}(t_m) = \boldsymbol{v}(t_m) - \boldsymbol{v}_{\text{Pl}}(t_m). \tag{28}$$

The actual semi-major axis is

$$a(t_m) = \frac{\mu_{\text{Pl}}}{\left(\dfrac{2\mu_{\text{Pl}}}{\Delta\boldsymbol{r}(t_m)} - \Delta v^2(t_m)\right)}. \tag{29}$$

The eccentricity vector is

$$\boldsymbol{e} = \frac{1}{\mu_{\text{Pl}}}\left[\left(\Delta\boldsymbol{v}(t_m)^2 - \frac{\mu_{\text{Pl}}}{\Delta\boldsymbol{r}(t_m)}\right)\Delta\boldsymbol{r}(t_m) - (\Delta\boldsymbol{r}(t_m) \cdot \Delta\boldsymbol{v}(t_m))\Delta\boldsymbol{v}(t_m)\right], \tag{30}$$

The perigee distance is therefore defined as

$$r_{\text{p}}(t_m) = a(1-e). \tag{31}$$

It is trivial to obtain the true anomaly; let us constrain the spacecraft at the perigee via a simple form at the inner time t_m, that is

$$\Delta\boldsymbol{r}(t_m) \times \Delta\boldsymbol{v}(t_m) = 0. \tag{32}$$

3.2.2 Second type of inner constraints

The concept of the B-plane is used to describe the hyperbolic relative to the GA. The second type of inner constraints is therefore given as

$$\psi^2_{13-15} \triangleq \begin{bmatrix} B_{\text{T}}(t_m) - B_{\text{Tnorm}} \\ B_{\text{R}}(t_m) - B_{\text{Rnorm}} \\ f(t_m) - f_{\text{norm}} \end{bmatrix} = 0, \tag{33}$$

where $B_{\text{T}}(t_m)$ and $B_{\text{R}}(t_m)$ are the actual B-plane parameters at t_m. B_{Tnorm} and B_{Rnorm} are the nominal B-plane parameters.

Figure 2 shows the hyperbolic trajectory and the B-plane relative to the planet, where $\boldsymbol{S}$ is the unit vector that has its origin at the target body's center of mass and is parallel to the incoming asymptote. The unit vectors $\boldsymbol{T}$ and $\boldsymbol{R}$ lay on the B-plane and have their origin at the target body's center of mass. $\boldsymbol{S}$, $\boldsymbol{T}$, and $\boldsymbol{R}$ constitute a right-handed Cartesian coordinate system. Let us set a reference unit vector $\boldsymbol{N}$ as the ecliptic plane normal, so $\boldsymbol{T}$ and $\boldsymbol{R}$ are defined as

$$\boldsymbol{T} = \boldsymbol{S} \times \boldsymbol{N}, \quad \boldsymbol{R} = \boldsymbol{S} \times \boldsymbol{T}, \tag{34}$$

and $\boldsymbol{B}$, B_{T}, and B_{R} can be defined as

$$\boldsymbol{B}_{\text{norm}} = b(\boldsymbol{S} \times \boldsymbol{n}), \quad B_{\text{T}} = \boldsymbol{B} \cdot \boldsymbol{T}, \quad B_{\text{R}} = \boldsymbol{B} \cdot \boldsymbol{R}. \tag{35}$$

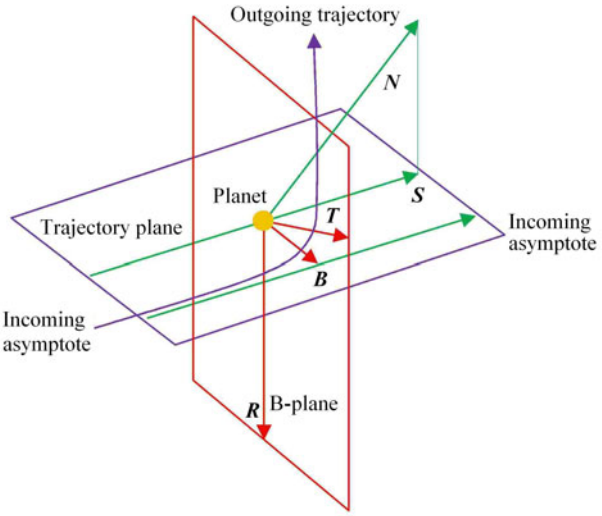

Fig. 2 B-plane

3.2.2.1 Nominal B-plane parameters

The nominal B-plane parameters can be defined by the incoming and outgoing hyperbolic excess velocities in the two-

body model with a GA. First, the normal of the hyperbolic trajectory is the same as Eq. (23), and the incoming asymptote unit vector can be defined as

$$\boldsymbol{S} = \boldsymbol{v}_{\infty}^{-}/v_{\infty}. \tag{36}$$

The semi-major axis and the semi-minor axis of the hyperbolic trajectory are defined as

$$a = -\frac{\mu_{\mathrm{Pl}}}{v_{\infty}^2}, \quad b = -a\cot\left(\frac{\theta}{2}\right), \tag{37}$$

where θ is the tuning angle of the hyperbolic excess speed for the planetary GA, and is defined as

$$\theta = 2\sin^{-1}\left[\left(1+\frac{v_{\infty}^2 r_{\mathrm{p}}}{\mu_{\mathrm{Pl}}}\right)^{-1}\right], \tag{38}$$

where r_{p} is the radius of the GA given by a two-body model, which is the same as r_{pnorm}.

Therefore, the nominal B-plane parameters can be obtained via Eqs. (35) and (36).

3.2.2.2 Actual B-plane parameters

The actual B-vector and B-plane parameters are given via the states of the spacecraft relative to the GA planet at the time of the perigee of the GA planet. First, the normal unit vector of the trajectory relative to the GA planet $\boldsymbol{n}$ is defined as

$$\boldsymbol{n} = \frac{\Delta\boldsymbol{r}(t_m)\times\Delta\boldsymbol{v}(t_m)}{\|\Delta\boldsymbol{r}(t_m)\times\Delta\boldsymbol{v}(t_m)\|}, \tag{39}$$

and the $\boldsymbol{S}$ vector, which can be calculated from $\Delta\boldsymbol{r}$ and $\Delta\boldsymbol{v}$, is defined as

$$\boldsymbol{S} = \frac{\boldsymbol{e}}{e}\cos\gamma + \frac{\boldsymbol{n}\times\boldsymbol{e}}{|\boldsymbol{n}\times\boldsymbol{e}|}\sin\gamma, \tag{40}$$

where $\boldsymbol{e}$ is the eccentricity vector and has the form of Eq. (37). B is defined as

$$\gamma = \cos^{-1}(1/e). \tag{41}$$

Therefore, the actual B-plane parameters can be obtained via Eq. (35).

3.3 Solving strategy summary

According to the transversal conditions, when the boundary state is fixed, the corresponding boundary costate is free, and when the former is free, the latter is fixed. The initial position and velocity constraints are time dependent, so the initial and final costate vectors should satisfy

$$\boldsymbol{\lambda}_r(t_0) = -\boldsymbol{\chi}_{1-3}, \quad \boldsymbol{\lambda}_v(t_0) = -\boldsymbol{\chi}_{4-6}, \tag{42}$$

$$\boldsymbol{\lambda}_r(t_{\mathrm{f}}) = \boldsymbol{\chi}_{7-9}, \quad \boldsymbol{\lambda}_v(t_{\mathrm{f}}) = \boldsymbol{\chi}_{10-12}, \tag{43}$$

$$\lambda_m(t_{\mathrm{f}}) = 0. \tag{44}$$

For convenience, in the numerical solution process, $\boldsymbol{\chi}_{1-12}$ is expressed with $\boldsymbol{\lambda}_r(t_0)$, $\boldsymbol{\lambda}_v(t_0)$, $\boldsymbol{\lambda}_r(t_{\mathrm{f}})$, and $\boldsymbol{\lambda}_v(t_{\mathrm{f}})$ via Eqs. (42) and (43). Therefore, the Lagrange numerical multipliers $\boldsymbol{\chi}_{1-12}$ do not appear in the shooting functions.

Similarly, the intermediate transversal conditions are

$$-\lambda(t_m^-) + \lambda(t_m^+) + \frac{\boldsymbol{\chi}_{13-15}\cdot\partial\boldsymbol{\psi}_{13-15}}{\partial x(t_m)} = 0. \tag{45}$$

The boundary stationary conditions are derived as

$$-H(t_0) - \boldsymbol{\chi}_{1-3}\cdot\boldsymbol{v}_{\mathrm{As1}}(t_0) - \boldsymbol{\chi}_{4-6}\cdot\boldsymbol{a}_{\mathrm{As1}}(t_0) = 0, \tag{46}$$

$$H(t_{\mathrm{f}}) - \boldsymbol{\chi}_{7-9}\cdot\boldsymbol{v}_{\mathrm{As2}}(t_{\mathrm{f}}) - \boldsymbol{\chi}_{10-12}\cdot\boldsymbol{a}_{\mathrm{As2}}(t_{\mathrm{f}}) = 0. \tag{47}$$

The inner stationary is

$$H(t_m^-) - H(t_m^+) + \frac{\boldsymbol{\chi}_{13-15}\cdot\partial\boldsymbol{\psi}_{13-15}}{\partial t_m} = 0. \tag{48}$$

If the initial time, the event time or the final time is fixed, then the corresponding stationary conditions will disappear.

The inner constraints are associated with an intermediate state and time. The remaining task is to calculate the derivatives of the inner constraints $\boldsymbol{\psi}_{13-15}$; in other words, the $i(t_m)$, $r_{\mathrm{p}}(t_m)$, and $f(t_m)$ or B_{T}, B_{R}, and $f(t_m)$ with respect to the basic variables $\boldsymbol{r}(t_m)$, $\boldsymbol{v}(t_m)$, and t_m.

With the inequality constraints and the two types of inner constraints above, after some complicated derivation and assembly, the relation of the inner constraints and the intermediate state and time is finally deduced. The form of the formula of the second type is very complicated, and thus this paper simply gives the derivation of the formula of the first type of the inner constraints.

For convenience, the "(t_m)" is omitted after the variables a, $\boldsymbol{e}$, e, i, $\boldsymbol{h}$, h, $\boldsymbol{r}$, r, $\boldsymbol{v}$, v, $\boldsymbol{B}$, $\boldsymbol{S}$, BT, and BR in the derivation; the values of all of these variables are assumed to be at t_m. First, let us find the derivatives of the first type of the inner constraints $\boldsymbol{\psi}^1$ to the basic variables $\boldsymbol{r}(t_m)$, $\boldsymbol{v}(t_m)$, and t_m.

The partial derivative with respect to $\boldsymbol{x}(t_m)$ of the cosine of the orbit inclination is

$$\frac{\partial(\cos i - \cos i_{\mathrm{norm}})}{\partial\boldsymbol{x}(t_m)} = -\frac{1}{h^3}\frac{\partial\boldsymbol{h}}{\partial\boldsymbol{x}(t_m)}\cdot\boldsymbol{h}\cdot\boldsymbol{h}^{\mathrm{T}}\cdot\boldsymbol{k} + \frac{1}{h}\frac{\partial\boldsymbol{h}}{\partial\boldsymbol{x}(t_m)}\cdot\boldsymbol{k}, \tag{49}$$

where $\boldsymbol{h}$ is a column vector and $\boldsymbol{h}^{\mathrm{T}}$ is a row vector. If the column vector $\boldsymbol{a} = (a_1, a_2, a_3)^{\mathrm{T}}$, $\tilde{\boldsymbol{a}}$ is denoted as

$$\tilde{\boldsymbol{a}} = \begin{bmatrix} 0 & -a_3 & a_2 \\ a_3 & 0 & -a_1 \\ -a_2 & a_1 & 0 \end{bmatrix}$$

and it can be easily seen that $\tilde{\boldsymbol{a}}^{\mathrm{T}} = -\tilde{\boldsymbol{a}}$. Then

$$\frac{\partial\boldsymbol{h}}{\partial\boldsymbol{x}(t_m)} = \frac{\partial(\Delta\boldsymbol{r}\times\Delta\boldsymbol{v})}{\partial\boldsymbol{x}(t_m)} = \frac{\partial\Delta\boldsymbol{r}}{\partial\boldsymbol{x}(t_m)}\cdot\Delta\tilde{\boldsymbol{v}} - \frac{\partial\Delta\boldsymbol{v}}{\partial\boldsymbol{x}(t_m)}\Delta\tilde{\boldsymbol{r}}, \tag{50}$$

and the partial derivative with respect to t_m of the cosine of the orbit inclination is

$$\frac{\partial(\cos i - \cos i_{\mathrm{norm}})}{\partial t_m} = -\frac{1}{h^3}\left(\frac{\partial\boldsymbol{h}}{\partial t_m}\cdot\boldsymbol{h}\right)\cdot\boldsymbol{h}(t_m)\cdot\boldsymbol{k} + \frac{1}{h}\frac{\partial\boldsymbol{h}}{\partial t_m}\cdot\boldsymbol{k}, \tag{51}$$

where

$$\frac{\partial\boldsymbol{h}}{\partial t_m} = \frac{\partial\Delta\boldsymbol{r}}{\partial t_m}\times\Delta\boldsymbol{v} + \Delta\boldsymbol{r}\times\frac{\partial\Delta\boldsymbol{v}}{\partial t_m}, \tag{52}$$

$$\frac{\partial \Delta \boldsymbol{r}(t_m)}{\partial t_m} = -\boldsymbol{v}_{\mathrm{pl}}(t_m), \quad \frac{\partial \Delta \boldsymbol{v}(t_m)}{\partial t_m} = -\boldsymbol{a}_{\mathrm{pl}}(t_m). \tag{53}$$

The partial derivative with respect to $\boldsymbol{x}(t_m)$ of the perigee distance is

$$\frac{\partial (r_{\mathrm{p}} - r_{\mathrm{pnorm}})}{\partial \boldsymbol{x}(t_m)} = (1-e)\frac{\partial a}{\partial \boldsymbol{x}(t_m)} - a\frac{\partial e}{\partial \boldsymbol{x}(t_m)}, \tag{54}$$

where

$$\frac{\partial a}{\partial \boldsymbol{x}(t_m)} = \frac{2\mu_{\mathrm{Pl}}}{\left(\frac{2\mu_{\mathrm{Pl}}}{\Delta r} - \Delta v^2\right)^2}\left(\frac{\mu_{\mathrm{Pl}}}{\Delta r^2}\frac{\partial \Delta \boldsymbol{r}}{\partial \boldsymbol{x}(t_m)} + \Delta v \frac{\partial \Delta \boldsymbol{v}}{\partial \boldsymbol{x}(t_m)}\right), \tag{55}$$

$$\frac{\partial e}{\partial \boldsymbol{x}(t_m)} = \frac{1}{e}\frac{\partial \boldsymbol{e}}{\partial \boldsymbol{x}(t_m)} \cdot \boldsymbol{e}, \tag{56}$$

where

$$\frac{\partial \Delta \boldsymbol{r}}{\partial \boldsymbol{x}(t_m)} = \frac{1}{\Delta r}\frac{\partial \Delta \boldsymbol{r}}{\partial \boldsymbol{x}(t_m)} \cdot \Delta \boldsymbol{r}, \quad \frac{\partial \Delta v}{\partial \boldsymbol{x}(t_m)} = \frac{1}{\Delta v}\frac{\partial \Delta \boldsymbol{v}}{\partial \boldsymbol{x}(t_m)} \cdot \Delta \boldsymbol{v}, \tag{57}$$

$$\begin{aligned}\frac{\partial e}{\partial \boldsymbol{x}(t_m)} = {} & \frac{1}{\mu_{\mathrm{Pl}}}\left(2\Delta v \frac{\partial \Delta v}{\partial \boldsymbol{x}(t_m)} + \frac{\mu_{\mathrm{Pl}}}{\Delta r^2}\frac{\partial \Delta r}{\partial \boldsymbol{x}(t_m)}\right)\Delta \boldsymbol{r}^{\mathrm{T}} \\ & + \frac{1}{\mu_{\mathrm{Pl}}}\left(\Delta v^2 - \frac{\mu_{\mathrm{Pl}}}{\Delta r}\right)\frac{\partial \Delta \boldsymbol{r}}{\partial \boldsymbol{x}(t_m)} - \frac{1}{\mu_{\mathrm{Pl}}}\left(\frac{\partial \Delta \boldsymbol{r}}{\partial \boldsymbol{x}(t_m)} \cdot \Delta \boldsymbol{v}\right)\Delta \boldsymbol{v}^{\mathrm{T}} \\ & - \frac{1}{\mu_{\mathrm{Pl}}}\left(\frac{\partial \Delta \boldsymbol{v}}{\partial \boldsymbol{x}(t_m)} \cdot \Delta \boldsymbol{r}\right)\Delta \boldsymbol{v}^{\mathrm{T}} - \frac{1}{\mu_{\mathrm{Pl}}}(\Delta \boldsymbol{r} \cdot \Delta \boldsymbol{v})\frac{\partial \Delta \boldsymbol{v}}{\partial \boldsymbol{x}(t_m)}.\end{aligned} \tag{58}$$

The partial derivative with respect to t_m of the perigee distance is

$$\frac{\partial (r_{\mathrm{p}} - r_{\mathrm{pnorm}})}{\partial t_m} = (1-e)\frac{\partial a}{\partial t_m} - a\frac{\partial e}{\partial t_m}, \tag{59}$$

where

$$\frac{\partial a}{\partial t_m} = \frac{2\mu_{\mathrm{Pl}}}{\left(\frac{2\mu_{\mathrm{Pl}}}{\Delta r} - \Delta v^2\right)^2}\left(\frac{\mu_{\mathrm{Pl}}}{\Delta r^2}\frac{\partial \Delta \boldsymbol{r}}{\partial t_m} + \Delta v \frac{\partial \Delta \boldsymbol{v}}{\partial t_m}\right), \tag{60}$$

$$\frac{\partial e}{\partial t_m} = \frac{1}{e}\frac{\partial \boldsymbol{e}}{\partial t_m} \cdot \boldsymbol{e}, \tag{61}$$

where

$$\frac{\partial \Delta \boldsymbol{r}}{\partial t_m} = \frac{1}{\Delta r}\frac{\partial \Delta \boldsymbol{r}}{\partial t_m} \cdot \Delta \boldsymbol{r}, \quad \frac{\partial \Delta v}{\partial t_m} = \frac{1}{\Delta v}\frac{\partial \Delta \boldsymbol{v}}{\partial t_m} \cdot \Delta \boldsymbol{v}, \tag{62}$$

$$\begin{aligned}\frac{\partial \boldsymbol{e}}{\partial t_m} = {} & \frac{1}{\mu_{\mathrm{Pl}}}\left(2\Delta v \frac{\partial \Delta v}{\partial t_m} + \frac{\mu_{\mathrm{Pl}}}{\Delta r^2}\frac{\partial \Delta \boldsymbol{r}}{\partial t_m}\right)\Delta \boldsymbol{r} \\ & + \frac{1}{\mu_{\mathrm{Pl}}}\left(\Delta v^2 - \frac{\mu_{\mathrm{Pl}}}{\Delta r}\right)\frac{\partial \Delta \boldsymbol{r}}{\partial t_m} - \frac{1}{\mu_{\mathrm{Pl}}}\left(\frac{\partial \Delta \boldsymbol{r}}{\partial t_m} \cdot \Delta \boldsymbol{v}\right)\Delta \boldsymbol{v} \\ & - \frac{1}{\mu_{\mathrm{Pl}}}\left(\frac{\partial \Delta \boldsymbol{v}}{\partial t_m} \cdot \Delta \boldsymbol{r}\right)\Delta \boldsymbol{v} - \frac{1}{\mu_{\mathrm{Pl}}}(\Delta \boldsymbol{r} \cdot \Delta \boldsymbol{v})\frac{\partial \Delta \boldsymbol{v}}{\partial t_m}.\end{aligned} \tag{63}$$

The partial derivative with respect to $\boldsymbol{x}(t_m)$ of the third of Eq. (21) is

$$\frac{\partial (\Delta \boldsymbol{r} \cdot \Delta \boldsymbol{v})}{\partial \boldsymbol{x}(t_m)} = \frac{\partial \Delta \boldsymbol{r}}{\partial \boldsymbol{x}(t_m)} \cdot \Delta \boldsymbol{v} + \frac{\partial \Delta \boldsymbol{v}}{\partial \boldsymbol{x}(t_m)} \cdot \Delta \boldsymbol{r}. \tag{64}$$

It is clear that there are 13 unknowns, including the 7-D initial values of the costate vectors $\boldsymbol{\lambda}(t_0)$, the 3-D initial time t_0, event time t_m, and final time t_{f}, and the 3-D numerical multipliers $\boldsymbol{X}_{13-15}$. At the same time, there are an identical number of equations, including the 6-D rendezvous conditions (20), the 1-D transversal condition (44), the 3-D stationary condition (46)–(48), and the 3-D inner constraint (21) or (33). It is important to note that the transversal conditions (45) are not used to constitute targeting functions but are used to update the value of the costate vectors at the event time t_m. The values of the position vectors, the velocity vectors and the mass of the spacecraft are continuous at the event time t_m, so they need not be updated.

4 Examples and results

Two examples of fuel-optimal problems with fixed boundary conditions with and without an intermediate GA in a full ephemeris model will be given to substantiate the techniques and theories presented in Sects. 2 and 3, respectively. The heliocentric position, velocity and orbit elements of the planets are computed online by the JPL Horizons system.

In the numerical results, a series of techniques is applied to enhance the possibility of convergence of the global optimal solution. First, by multiplying the performance index by a positive unknown factor, the optimal control problem can be made homogeneous to the Lagrange multipliers including this factor. Hence, normalization can restrict the unknown multipliers on a unit hypersphere. Second, an integration rule using the Runge–Kutta algorithm with a fixed step is constructed to guarantee the accuracy for the bang-bang control; in addition, the switching function's first- and second-order derivatives with respect to time are derived to predict the thrust trend. Third, a homotopic approach that solves the fuel-optimal problem of a low-thrust trajectory by starting from the related and easier energy-optimal problem is applied.

For calculation convenience, the quantities of length, time, and mass are normalized by the astronomy unit (AU, 149 597 870.66 km), a year (a, $356.25 \times 86\,400$ s), and the initial spacecraft mass (m_0), respectively. Therefore, the value of μ should be 39.476 926 $\mathrm{AU}^3/\mathrm{a}^2$, and the other values should be made consistent with the normalized units.

4.1 Rendezvous problem from the sphere of influence of Earth to Apophis

The mass of the spacecraft, the specific impulse of the electric propulsion system, and other parameters are given in Table 1.

The rendezvous problem from Earth to Apophis is considered; in this problem, the spacecraft starts with the hyperbolic excess velocity vector $\boldsymbol{v}_\infty$ provided by the launch

Table 1 The values of the parameters of the spacecraft

m_0/kg	$T_{\max}$/mN	I_{sp}/s	η	S/m^2	$L_0/(\mathrm{N{\cdot}km}^2)$	J_2
1 750	160	1 600	0.37	26.78	3.03×10^{25}	$1\,082.63 \times 10^6$

vehicle at a parking orbit, flies through Earth's sphere of influence, and finally arrives at Apophis with the same heliocentric position and velocity. For simplicity, the initial time t_0, the final time t_f and the boundary value are fixed. The example therefore becomes a TPBVP. The boundary value is listed in Table 2.

Table 2 The boundary value of the mission

Parameter	Value
Initial time (MJD)	58 051.021
Initial position/km	[127 477 808.816; 783 369 336.728; −354 430 668.107]
Initial velocity/(km·s^{-1})	[−12.719 331; 27.696 476; −1.685 359]
Final time (MJD)	58 964.979
Final position/km	[−160 034 368.427; 248 741 925.082; −5 126 777.683]
Final velocity/(km·s^{-1})	[−1.935 541; −25.903 673; 1.333 462]

The techniques and the solving strategy presented in Sect. 2 are applied to solve this fuel-optimal rendezvous problem. In the process of optimizing the low-thrust trajectory, because the ephemeris data are read frequently, the time spent on the numerical calculation with the full ephemeris model is longer than that with the two-body model. To improve the computational efficiency, the low-thrust trajectory optimization with the two-body model is solved first, and then the solution is set as the initial value of the costate vectors for the problem with the full ephemeris model.

Figure 3 shows the transfer trajectory with both the two-body model and the full ephemeris model. Figure 4 shows the optimal magnitude of the thrust for both the two-body model and the full ephemeris model, and the boot and shutdown sequence is listed in Table 3. Both models have identical boot and shutdown sequences, but the time is slightly different. The fuel consumption is 221.4 kg in the full ephemeris model, which is close to the fuel consumption of 221.3 kg in the two-body model. Figure 5 shows the control history in the two-body model and the full ephemeris model. Through the contract, it is clear that the two-body model is reasonable in the initial design of the trajectory, and the result of the fuel consumption has a high reference value. However, in practical engineering, the result designed with the full ephemeris model has to be used.

Figure 6 shows the changing trend of various main perturbations during the spacecraft's flight, which represents typical perturbative conditions of the spacecraft near the Earth. The units of the vertical axis are km/s^2, the magnitude of the central force of the Sun's gravity is 5×10^{-6} km/s^2, and the magnitude of the force of the electric propulsion system is 9×10^{-8} km/s^2. The figure shows that the main perturbations are Earth's and the Moon's gravities when the craft is just leaving Earth. The main perturbations become the solar radiation pressure and Earth's gravity in the cruising flight, and Jupiter's and Venus's gravities can not be ignored.

4.2 Rendezvous problem from Apophis to 1996FG3

The mass of the spacecraft, the specific impulse of the electric propulsion system, and other parameters are given in Table 4.

Table 3 The boot and shutdown sequence

Sequence	Full ephemeris model	Two-body model
Departing from Earth	58 051.021	58 051.021
Turning on the electric propulsion system	58 203.024	58 203.476
Shutting off the electric propulsion system	58 206.280	58 206.974
Turning on the electric propulsion system	58 543.289	58 543.743
Shutting off the electric propulsion system	58 677.023	58 676.682
Turning on the electric propulsion system	58 718.982	58 718.869
Shutting off the electric propulsion system	58 778.684	58 778.596
Turning on the electric propulsion system	58 910.433	58 909.972
Targeting Apophis	58 964.979	58 964.979

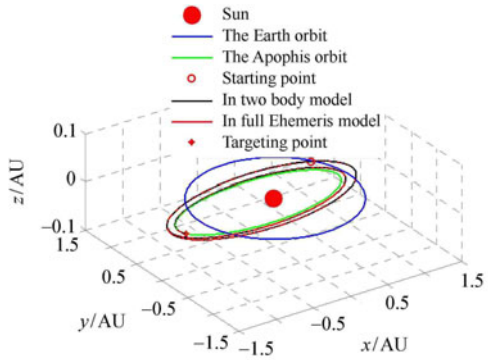

Fig. 3 Heliocentric orbit in the two-body model and the full ephemeris model

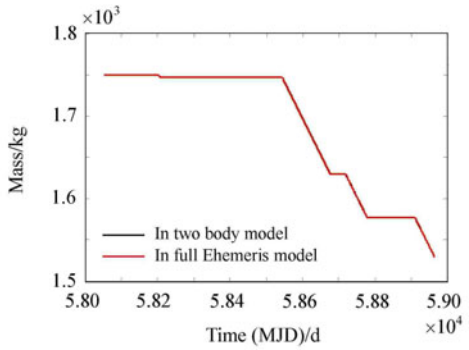

Fig. 4 Fuel consumption rate in the two-body model and the full ephemeris model

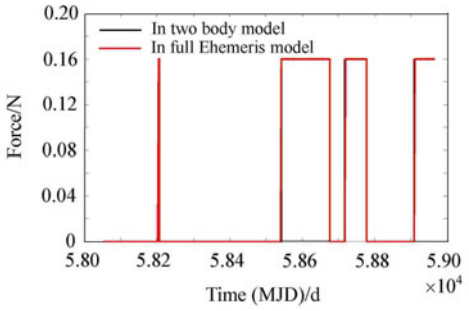

Fig. 5 Control history in the two-body model and the full ephemeris model

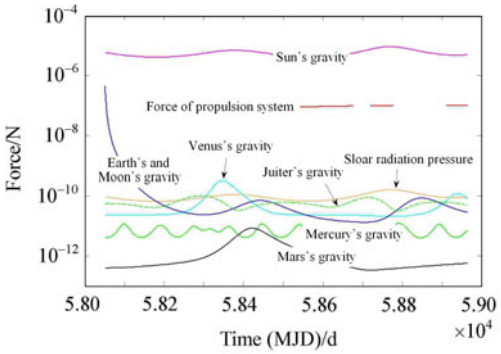

Fig. 6 The magnitudes of various forces in the full ephemeris model

Table 4 The values of the parameters of the spacecraft

m_0/kg	T_{max}/mN	I_{sp}/s	η	S/m^2	L_0/(N·km^2)	J_2
2 000	40	1 600	0.37	26.78	3.03×10^{25}	$1\,082.63\times10^{6}$

The rendezvous problem from Apophis to 1996FG3 via an Earth GA with the full ephemeris model is considered. In this problem, the spacecraft starts with the Apophis heliocentric position and velocity and arrives at 1996FG3 with the same heliocentric position and velocity of 1996FG3. This example, which avoids the escaping orbit and the capture orbit, is chosen to highlight the core technique presented in Sect. 3. It hardly matters, which is not because the effect of the GA is not very significant in this example, but is because the difference discussed here is between the optimization using the two-body model and using the full ephemeris model for GA, rather than between the low-thrust trajectory optimization with and without GA. The boundary value is listed in Table 5.

Table 6 lists the result designed via the two-body model, including the initial time, the final time, the hyperbolic excess velocity $\boldsymbol{v}_\infty^-$, $\boldsymbol{v}_\infty^+$, and the rotation angle δ_0, among others. The nominal orbit inclination and the perigee distance are calculated from these values via the formula given in Sect. 3. All the vectors are projected into the HECS.

Table 5 The boundary value of the mission

Parameter	Value
Initial time (MJD)	59 731.267
Initial position/km	[63 961 111.513; −93 560 609.112; 6 499 338.545]
Initial velocity/(km·s^{-1})	[29.036 008; 23.084 452; −0.524 435]
Final time (MJD)	60 357.404
Final position/km	[−159 321 689.607; 140 531 008.822; −2 374 517.803]
Final velocity/(km·s^{-1})	[−14.064 768; −14.480 514; −0.674 215]

Because of the highly nonlinear, highly sensitive initial values of the costate vectors in the fuel-optimal problem with the full ephemeris model, the first half of the mission has to be solved, which starts from Apophis and arrives at the GA planet, Earth. In this problem, the initial state and the starting time are identical to those above, and the final boundary value is the same as the inner constraints of the whole mission. The solution of the two-body model is given for the equation of the first half of the mission, and then the solution of the first half is given for the whole mission. A fixed step is used in the switching detection integration method and the homotopic approach. Approximately one week is required to obtain the solutions of the whole mission using the full ephemeris model. The result is listed in Table 7.

Table 6 The result designed via the two-body model

Variables	Value
Event (MJD)	60 078.339
The incoming hyperbolic excess velocity $\boldsymbol{v}_{\infty}^{-}/(\mathrm{km{\cdot}s^{-1}})$	$[2.164\,069,\ 8.946\,526,\ 1.201\,325]^{\mathrm{T}}$
The outgoing hyperbolic excess velocity $\boldsymbol{v}_{\infty}^{+}/(\mathrm{km{\cdot}s^{-1}})$	$[3.120\,867,\ 8.737\,213,\ 0.296\,646]^{\mathrm{T}}$
The velocity increment $\Delta\boldsymbol{v}_{\mathrm{GA}}/(\mathrm{km{\cdot}s^{-1}})$	$[0.956\,798,\ -0.209\,313,\ -0.904\,679]^{\mathrm{T}}$
The rotation angle $\delta_0/(^\circ)$	8.237
The fuel consumption Δm/kg	567.98
The nominal value designed via the two-body model $\cos i_0$	−0.730 113
The nominal value designed via the two-body model $r_{\mathrm{p}0}$	59 785.98

Table 7 The result designed with the full ephemeris model

Variables	Value
The time entering the sphere of influence of Earth t_{m0} (MJD)	60 077.210
The incoming hyperbolic excess velocity $\boldsymbol{v}_{\infty}^{-}/(\mathrm{km{\cdot}s^{-1}})$	$[2.163\,688,\ 8.974\,275,\ 1.203\,794]^{\mathrm{T}}$
The perigee time t_m (MJD)	60 078.339
The time leaving the sphere of influence of Earth t_{m0} (MJD)	60 079.467
The outgoing hyperbolic excess velocity $\boldsymbol{v}_{\infty}^{+}/(\mathrm{km{\cdot}s^{-1}})$	$[3.125\,561,\ 8.765\,581,\ 0.267\,808]^{\mathrm{T}}$
The fuel consumption Δm/kg	567.40

Figure 7 shows the transfer trajectory in the HOCS. Figure 8 shows the trajectory near the Earth when it receives a GA. In the full ephemeris model, the spacecraft flies through the sphere of influence of Earth for two days, and the GA trajectory near Earth is obtained. In the two-body model, however, the trajectory flies through the center of Earth at the event time and obtains the velocity increment instantaneously, which can not describe the GA trajectory.

Figures 9 and 10 give the fuel consumption rate and the control history both for the two-body model and for the full ephemeris model, which are close to each other. Table 8 lists the boot and shutdown sequence.

Figure 11 shows the main force and perturbations during the flight. As in the first example, the spacecraft flies closely by the GA planet, and the spacecraft is subject to perturbations throughout the flight, especially the solar radiation pressure and the gravities of Venus and Jupiter.

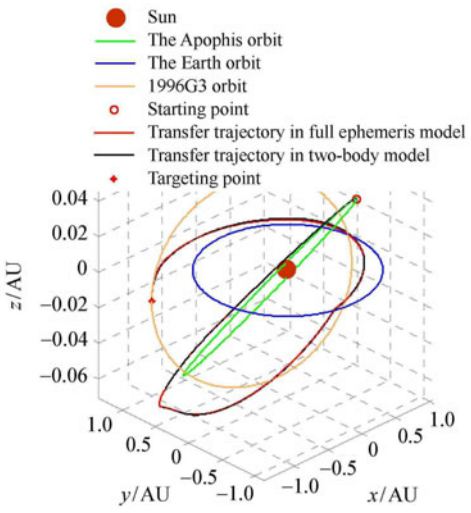

Fig. 7 Heliocentric trajectory in the two-body model and the full ephemeris model

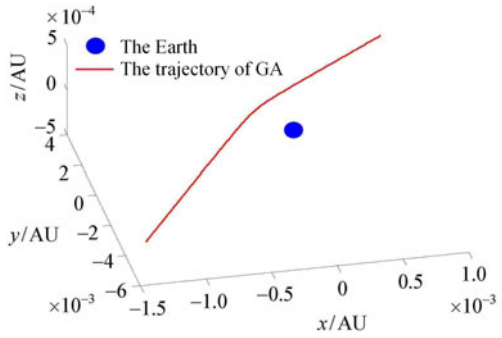

Fig. 8 Heliocentric trajectory near the Earth

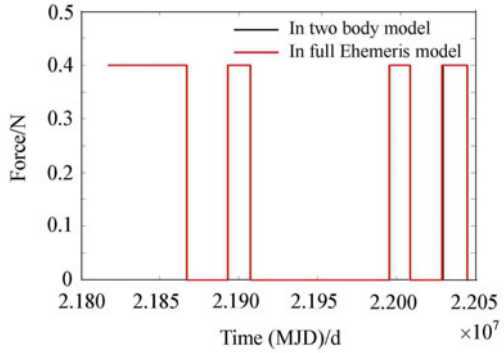

Fig. 10 Control history in the two-body model and the full ephemeris model

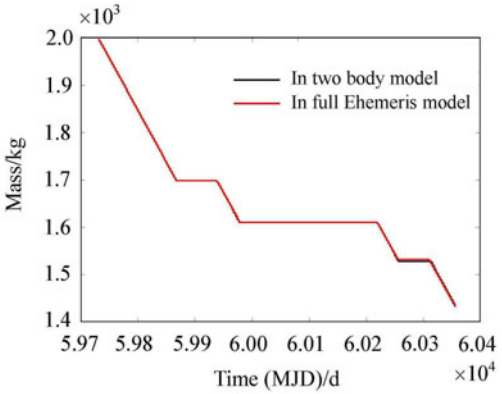

Fig. 9 Fuel consumption rate in the two-body model and the full ephemeris model

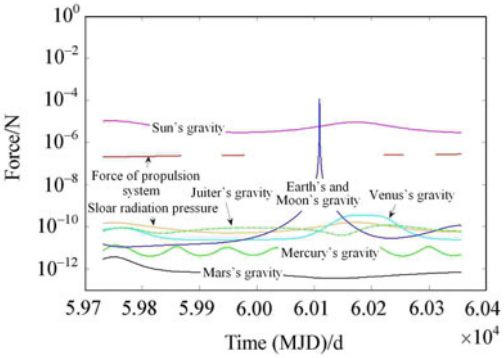

Fig. 11 The magnitude of various forces in the full ephemeris model

Table 8 The boot and shutdown sequence

Sequence	Full ephemeris model	Two-body model
Departing from Apophis	59 731.267	59 731.267
Shutting off the electric propulsion system	59 868.402	59 868.382
Turning on the electric propulsion system	59 939.324	59 939.181
Shutting off the electric propulsion system	59 979.444	59 979.564
Turning on the electric propulsion system	60 220.562	60 220.410
Shutting off the electric propulsion system	60 256.127	60 257.203
Turning on the electric propulsion system	60 311.355	60 313.876
Targeting 1996FG3	60 357.404	60 357.404

By analyzing the curve of the fuel consumption and the control history, the trajectory, the boot and the shutdown sequence and the fuel consumption are similar to the results obtained from the two-body model. The result designed via the two-body model is therefore reasonable and convincing.

Figures 12 and 13 show the change of mechanical energy during the trajectory both in the two-body model and the full ephemeris model, especially during the process of GA. From the figure, because of the Earth's gravity, the mechanical energy of the spacecraft increases when it is approaching the Earth in the full ephemeris model. However, the mechanical energy decreases when the spacecraft leaves the Earth because the gravity of the Earth becomes a resistance. The change of the mechanical energy can exactly describe the entire process in the full ephemeris model. Due to the GA of Earth, the mechanical energy increases from approximately $-280\,\mathrm{km}^2/\mathrm{s}^2$ before the GA to approximately $-260\,\mathrm{km}^2/\mathrm{s}^2$ after the GA. The mechanical energy remains the same during the rest of trajectory after leaving Earth.

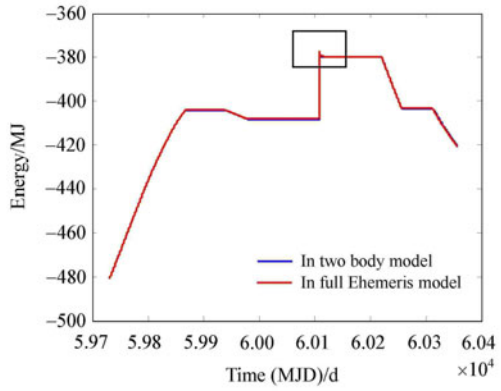

Fig. 12 Energy-changing curve in the full ephemeris model

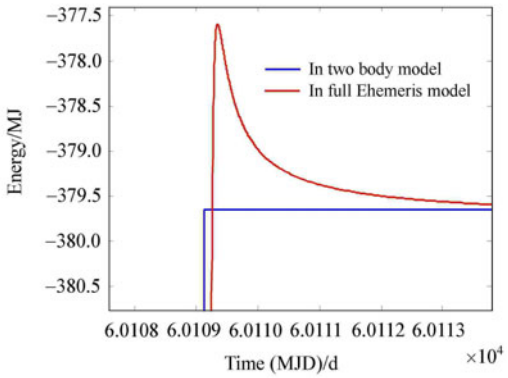

Fig. 13 Energy-changing curve at GA point in the full ephemeris model

5 Conclusion

The low-thrust trajectory optimization using a full ephemeris model is discussed, in which various perturbations, including a third-body's gravity perturbation, the solar radiation pressure and the nonspherical perturbation, are introduced into the dynamic equation. Compared with the central force and the force of electric propulsion, the perturbation is tiny, and the solution including the control history and the fuel consumption rate shows little difference. Because the ephemeris data are read frequently, the time spent on the numerical calculation with the full ephemeris model is longer than that with the two-body model.

In the full ephemeris model with GA, because the GA planet can not be modeled as a massless point, two sets of new equivalent inner constraints, which can accurately describe the GA process, are built to achieve the GA effect. The solutions including the control history and the fuel consumption rate of both models show little difference. Because the spacecraft flies through the GA planet's sphere of influence during the flight, the perturbation of the GA planet is obvious, the nonlinearity of the shoot function is enhanced, the domain of convergence becomes narrower, the initial values of the costate vectors become more sensitive, and the solution of the shooting function becomes much harder to obtain; in addition, the time spent on solving the shoot function dozens of times longer than that using the two-body model, even if the homotopic approach is used.

Comparing the two-body model and the full ephemeris model, the design results both with and without GA show that the solutions of both models show little difference, and thus the two-body model has a high reference value. For a practical mission, the preliminary design using the two-body model is therefore reasonable, and its precision can be reliably improved in the subsequent design by using the full ephemeris model.

References

1 Li, J., Jiang, F.: Survey of low-thrust trajectory optimization methods for deep space exploration. Mechanics Engineering **33**, 1–6 (2011)
2 Gao, Y.: Interplanetary travel with electric propulsion: technological progress, trajectory design, and comprehensive optimization. Chinese Journal of Theoretical and Applied Mechanics **43**, 991–1019 (2011)
3 Rayman, M.D., Fraschetti, T.C., Raymond, C.A.: Dawn: A mission in development for exploration of main belt asteroids Vesta and Ceres. Acta Astronautica **58**, 65–616 (2006)
4 Kuninaka, H., Nishivama, K., Funakai, I., et al: Asteroid rendezvous of HAYABUSA explorer using microwave discharge ion engines. In: The Proc. of the 29th International Electric Propulsion Conference, Oct. 31– Nov. 4, Princeton University, Princeton (2005)
5 Li, J., Baoyin, H.: Dynamics and control in deep space exploration. Mechanics Engineering **29**, 1–8 (2007)
6 Hargraves, C.R., Paris, S.W.: Direct trajectory optimization using nonlinear programming and collocation. Journal of Guidance, Control, and Dynamics **10**, 338–342 (1987)
7 Enright, P.J., Conway, B.A.: Discrete approximations to optimal trajectories using direct transcription and nonlinear programming. Journal of Guidance, Control, and Dynamics **15**, 994–1002 (1992)
8 Kechichian, J.A.: Optimal low-Earth-orbit-geostationary-Earth-orbit intermediate acceleration orbit transfer. Journal of Guidance, Control, and Dynamics **20**, 803–811 (1997)
9 Ranieri, C.L., Ocampo, C.A.: Indirect optimization of three-dimensional finite-burning interplanetary transfers including spiral dynamics. Journal of Guidance, Control, and Dynamics **32**, 444–454 (2009)
10 Kluever, C.A., Pierson, B.L.: Optimal low-thrust three-dimensional Earth-Moon trajectories. Journal of Guidance, Control, and Dynamics **18**, 830–837 (1995)
11 Gao, Y., Kluever, C.A.: Low-thrust interplanetary orbit transfers using hybrid trajectory optimization method with multiple shooting. AIAA/AAS Astrodynamics Specialist Conference and Exhibit, 16-19 August 2004, Providence, Rhode Island (2004)
12 Haberkorn, T., Martinon, P., Gergaud, J.: Low-thrust minimum-fuel orbital transfer: A homotopic approach. Journal of Guidance, Control, and Dynamics **27**, 1046–1060 (2004)

13 Martinon, P., Gergaud, J.: Using switching detection and variational equations for the shooting method. Optimal Control Applications and Methods **28**, 95–116 (2007)
14 Thevenet, J., Epenoy, R.: Minimum-fuel deployment for spacecraft formations via optimal control. Journal of Guidance, Control, and Dynamics **31**, 101–113 (2008)
15 D'Amario, L.A., Bright, L.E., Wolf, A.A.: Galileo trajectory design. Space Science Reviews **60**, 23–78 (1992)
16 Broucke, R.A.: The celestial mechanics of gravity assist. AIAA/AAS Astrodynamics Conference, Minneapoils, USA, Aug. 15–18 (1988)
17 Prado, A.F.B.: Powered swingby. Journal of Guidance, Control, and Dynamic **19**, 1142–1147 (1996)
18 Felipe, G., Prado, A.F.B.: Classification of out-of-plane swingby trajectories. Journal of Guidance, Control, and Dynamic **22**, 643–649 (1999)
19 Felipe, G., Prado, A.F.B.: Trajectory selection for a spacecraft performing a two-dimensional swing-by. Advances in Space Research **34**, 2256–2261 (2004)
20 Strange, N.J., Longuski, J.M.: Graphical method for gravity-assist trajectory design. Journal of Spacecraft and Rockets **30**, 9–16 (2002)
21 Bayliss, S.: Precision targeting for multiple swing by interplanetary trajectories. Journal of Spacecraft and Rockets **8**, 927–931 (1971)
22 Hull, D.G.: Conversion of optimal control problems into parameter optimization problems. Journal of Guidance, Control, and Dynamics **20**, 57–60 (1997)
23 Jiang, F., Baoyin, H., Li, J.: Practical techniques for low-thrust trajectory optimization with homotopic approach. Journal of Guidance, Control, and Dynamics **35**, 245–258 (2012)